Novel miRNA-inducing drugs enable differentiation of retinoic acid-resistant neuroblastoma cells

Lien D. Nguyen[1], Satyaki Sengupta[2], Kevin Cho[1], Alexander Floru[2], Rani E. George[2], and Anna M. Krichevsky[1,*]

Affiliation

1. Department of Neurology, Brigham and Women's Hospital and Harvard Medical School, Boston, MA 02115, USA

2. Department of Pediatric Oncology, Dana-Farber Cancer Institute and Harvard Medical School, Boston, MA, 02115, USA

*Correspondence: akrichevsky@bwh.harvard.edu

Keywords: Neuroblastoma, differentiation therapy, miR-124, MES, ADRN

Abstract

Tumor cell heterogeneity in neuroblastoma, a pediatric cancer arising from neural crest-derived progenitor cells, poses a significant clinical challenge. In particular, unlike adrenergic (ADRN) neuroblastoma cells, mesenchymal (MES) cells are resistant to chemotherapy and retinoid therapy and thereby significantly contribute to relapses and treatment failures. Previous research suggested that overexpression or activation of miR-124, a neurogenic microRNA with tumor suppressor activity, can induce the differentiation of retinoic acid-resistant neuroblastoma cells. Leveraging our established screen for miRNA modulatory small molecules, we validated PP121, a dual inhibitor of tyrosine and phosphoinositide kinases, as a robust inducer of miR-124. A combination of PP121 and miR-132-inducing bufalin synergistically arrests proliferation, induces differentiation, and prolongs the survival of differentiated MES SK-N-AS cells for 8 weeks. RNA-seq and deconvolution analyses revealed a collapse of the ADRN core regulatory circuitry (CRC) and the emergence of novel CRCs associated with chromaffin cells and Schwann cell precursors. Using a similar protocol, we differentiated and maintained other MES neuroblastoma, as well as glioblastoma cells, over 16 weeks. In conclusion, our novel protocol suggests a promising treatment for therapy-resistant cancers of the nervous system. Moreover, these long-lived, differentiated cells provide valuable models for studying mechanisms underlying differentiation, maturation, and senescence.

Introduction

Neuroblastoma, a cancer originating from neural crest cells (NCCs) and the most common extracranial solid tumor of childhood, exhibits remarkable diversities in clinical presentations, treatment responses, prognosis, and tumor characteristics. Patients classified as low/immediate risk have an excellent 5-year survival rate of above 95%, whereas the survival rate for patients classified as high risk remains below 50% (*1*). Cell lines derived from neuroblastoma tumors also display diversity in morphology, with earlier studies characterizing them as "N" cells, which have small, rounded cell bodies and numerous neurite-like processes, and "S" cells, which are larger, flattened, and highly substrate-adherent (*2, 3*). Next-generation sequencing techniques have enabled the classification of neuroblastoma cells into two genetically distinct groups: the adrenergic (ADRN) cells, which are lineage-committed, and the more immature mesenchymal (MES) cells, which more closely resemble NCCs (*4, 5*). ADRN and MES cells can interconvert into one another *in vitro* based on the switching of core regulatory circuitries (CRCs) (*5-7*). Notably, MES cells are generally resistant to standard treatments, including chemotherapy (*4, 5*), retinoic acid (RA) (*4*), inhibitors targeting anaplastic lymphoma kinase (ALK) (*8*), and therapeutic antibodies targeting disialoganglioside (GD2) (*9*). Furthermore, MES gene signature is enriched in relapsed tumors, suggesting that either ADRN cells convert to MES cells to escape treatments or that surviving MES cells repopulate new tumors (*10*). Overall, multiple evidence suggest an urgent need for treatments that effectively target MES neuroblastoma cells.

MicroRNAs (miRNAs) are small, noncoding RNAs that regulate gene expression by silencing mRNA targets. They play crucial roles in various cellular processes, including determining cell fate and identity (*11*). Particularly, miR-124 is one of the most enriched and abundant miRNAs in the nervous system and drives neuronal differentiation and neurite outgrowth (*12-15*). miR-124 is frequently downregulated in various types of cancers and is proposed as a key tumor suppressor targeting oncogenes and signaling pathways implicated in cancer progression (*16*). Multiple studies found that miR-124 was upregulated in neuroblastoma SH-SY-5Y cells differentiated by RA (*17-20*). Transfection of miR-124 mimics also drove neuronal differentiation in various neuroblastoma cell lines (*12, 21*). Therefore, we hypothesized that upregulation of miR-124 would promote the differentiation of neuroblastoma cells.

We previously developed a high-throughput screen for small molecule compounds that modulate neuronal miRNomes and established the first resource for miRNA-modulating drugs (*22, 23*). In this study, we leveraged this resource to test whether miR-124-inducing compounds inhibit proliferation and drive differentiation, particularly in RA-resistant MES cell lines. We validated PP121, a dual inhibitor of tyrosine and phosphoinositide kinases (*24*), as a robust activator of miR-124. In combination with bufalin, a drug that upregulates miR-132 and activates the BDNF pathway (*22*), PP121 completely arrested cell proliferation, promoted cell elongation, sprouting of neurite-like processes, and sustained cell survival for up to 8 weeks. Transcriptomic analyses revealed a permanent downregulation of cell cycle pathways, an upregulation of immune-related and senescence pathways, and, unexpectedly, an enhanced MES signature and decreased ADRN signature. Similar to observations made in RA-induced differentiation models (*25*), PP121/bufalin treatment led to a collapse of the ADRN CRC. In contrast to RA models, the retino-sympathetic

CRC that supports the RA-differentiated state was also downregulated following treatment. Instead, SK-N-AS cells differentiated towards a state that transcriptionally resembled chromaffin cells and Schwann cell precursors (SCPs) (*26*). We further showed that PP121 and bufalin also similarly differentiate additional MES neuroblastoma cell lines including GIMEN and SH-EP, and the glioblastoma LN-229 and U-251 cells. In summary, our study presents a novel method for differentiating neuroblastoma cells and supports a potential new avenue for the treatment of MES neuroblastomas resistant to standard therapies.

RESULTS

PP121 upregulates miR-124, arrests proliferation, and promotes neurite-like processes in SK-N-AS cell

Although previous studies implicated miR-124 in neuroblastoma differentiation (*12, 21*) , we first wanted to establish a causal relationship between miR-124 and differentiation in our cell line models. In humans, there are three miR-124 loci on chromosomes 2, 3, and 15 (*27*) that are processed into identical mature transcripts, with miR-124-3p being the major product. To determine whether exogenous miR-124 induces differentiation of MES neuroblastoma cells (*12, 21*), we transfected SK-N-AS cells with three miR-124-3p mimics corresponding to the three loci. We selected SK-N-AS cells because of their MES (*5*) or mixed identity (*4*), and resistance to RA-induced neuronal differentiation (*28, 29*). 4 days after transfection, live cell imaging revealed the emergence of rare neuron-like cells characterized by narrow, rounded cell bodies and neurite-like processes in all miR-124 transfected conditions, which were absent in cells transfected with control (CTRL mimics) (Fig. 1A). miR-124-transfected cells also showed a ~25% reduction in cell viability (Fig. 1B) and a ~40% reduction in confluence (Fig. 1C), suggesting that exogenous miR-124 reduced cell proliferation and drove some cells towards acquiring a differentiated morphology

Based on these observations, we hypothesized that endogenous induction of miR-124 in SK-N-AS cells would reduce proliferation and push cells toward a differentiated state. We proceeded to select 22 candidates with high miR-124-3p and -5p Z-scores from our previous dataset (Supp. Fig. 1A, Supp. Table 1) (*22*). We treated SK-N-AS cells with 22 candidate compounds and RA at 4 doses (0.3, 1, 3, and 10 µM; N=1 well per dose) and determined cell growth rate and morphological changes using the IncuCyte® imaging system (Fig. 1D-E, Supp. Table 2). Notably, cells treated with 3 or 10 µM PP121, a multikinase inhibitor, stopped proliferation, elongated, and sprouted neurite-like processes (Fig. 1D, Supp. Fig. 1B). 10 µM RA, which was sufficient to induce differentiation in various ADRN cell lines (*25, 30*), slightly reduced growth (Fig. 1E), but did not differentiate SK-N-AS cells (Supp. Fig. 1B). Next, to determine whether PP121's regulation of cell growth and morphology was associated with concomitant changes in miR-124 levels, we measured miR-124 abundance following treatment with increasing concentration of the compound for 7 days. Indeed, PP121 upregulated miR-124 levels in a dose-dependent manner over 7 days, with maximal upregulation observed at 5 uM (Fig. 1F). In line with this observation, 5 uM PP121 differentiated SK-N-AS cells (Supp. Fig. 1C). However, the same concentration of PP121 completely killed ADRN-type Kelly and SK-N-SH cells (Supp. Fig. 1C). 5 uM PP121 did not appear to kill primary rat neurons, suggesting that PP121 primarily affected proliferating cells

(Supp. Fig. 1C). Furthermore, the transformation of SK-N-AS cells by PP121 was reversible, as the removal of PP121 caused cells to again proliferate (Supp. Fig. 1D).

A novel protocol of PP121/bufalin induces long-term SK-N-AS differentiation.

As the morphologies of SK-N-AS cells treated with PP121 resembled the morphologies of RA-induced SH-SY-5Y differentiation, we tested an established protocol for SH-SY-5Y differentiation (*30*) (Supp. Fig. 2A). However, cells switched to neurobasal + 5 µM PP121 eventually clumped after several days, which were not ameliorated by adding BDNF, KCl, and db-cAMP (Supp. Fig. 2B). We and others previously found that cardiac glycosides activated the BDNF pathway in neurons (*22, 31*). Therefore, we tested a range of bufalin concentrations from 10 nM to 300 nM. Concentrations of 100 nM bufalin and above completely prevented cell clumping while further promoting the sprouting of neurite-like processes. Unexpectedly, with no medium change, cells treated with 100 nM bufalin survived mostly intact for 4 weeks, whereas higher concentrations led to cell degeneration and death (Supp. Fig. 2B). Other cardiac glycosides, including oleandrin (100 nM), digoxin (100 nM), and proscillaridin A (3 nM), also prevented clumpings, promoted neurite-like processes, and sustained cell viability over 4 weeks (Supp. Fig. 2C).

Next, we finalized a novel differentiation protocol involving 3 steps. First, SK-N-AS cells were plated at ~10% confluence and allowed to proliferate in DMEM, 10% FBS to ~30% confluence over 3 days. The medium was then switched to DMEM, 1% FBS, 5 µM PP121 for 4 days in stage 1 (S1). Finally, the medium was switched to neurobasal, 1X B27, 0.25X Glutamax, 5 µM PP121, and 100 nM bufalin in stage 2 (S2). New medium (20% of the initial volume) was added weekly to replace the evaporated medium (Fig. 2A). To determine how long the differentiated cells could survive, we imaged them continuously every 4 h for 8 weeks (Fig. 2B, Supp. Fig. 3A, supplementary video). Differentiated cells appeared mostly healthy for up to 4 weeks, with signs of degeneration slowly accumulating over the next 4 weeks. Intriguingly, over time, two distinct populations of cells emerged: a majority of non-motile, adherent, senescent-like cells and a minority of highly motile, poorly adherent, neuron-like cells that switched back and forth (Fig. 2B, C, Supp. Fig. 3B, supplementary video). Compared to naïve cells, immunostaining of S2D14 cells revealed a complete disappearance of the proliferation marker MKI67 (Fig. 2C, D) and an increase in TUJ1+ process length (Fig. 2C, E), suggesting that they had become differentiated cells.

PP121/bufalin inhibits proliferation but activates a non-neuronal differentiation

To understand the molecular mechanisms contributing to the differentiation of SK-N-AS cells, we performed RNA-seq analyses on 4 groups of samples (N=4 each): naive, S1D4, S2D4, and S2D30. Compared to naïve cells, differentiated cells showed a progressive downregulation of specific genes (such as TOP2A and MKI67) and pathways involved in cell proliferation (Fig. 3A-C) This pattern was in line with the observed cell proliferation arrest. Interestingly, PRRX1, a transcription factor (TF) associated with MES cells (*5, 6, 32*), was the second most significantly upregulated gene between naïve and S1D4 cells (Fig. 3A). In contrast, PHOX2A and PHOX2B, TFs associated with ADRN cells, were progressively downregulated in stage 2 (Fig. 3B-C). Unexpectedly, genes associated with neuronal states, such as MAP1A and SYP, were also downregulated in stage 2. Genes associated with inflammation, such as CCL3 and CCL3L3, were upregulated (Fig. 3B-C).

To understand the trajectory of differential gene expressions, we clustered normalized gene expression into 6 clusters (Fig. 3D, Supp. Table 3) and analyzed each cluster for Reactome pathway enrichment (Fig. 3E-J). Cluster 1, which was progressively downregulated over time, was enriched for pathways associated with Cell Cycle, Translation, and Metabolism of RNA (Fig. 3E), supporting the observation of complete arrest of cell proliferation. Cluster 2 (Fig. 3F), containing genes upregulated at S1D4, was enriched for the Interaction of L1 and ankyrins, which is associated with neurite outgrowth (*33*). Cluster 3 (Fig. 3G), containing genes upregulated at S2D4, was enriched for the RHO GTPase Cycle, which regulates many pathways, including cytoskeleton reorganization and cell adhesion (*34*). Cluster 4 (Fig. 3H), containing genes upregulated at S2D30, was enriched for Immune System and Neutrophil Degranulation, suggesting an increased inflammatory state. Cluster 5 (Fig. 3I), for genes upregulated in both S2D4 and S2D8, was enriched for Immune System. Interestingly, Signal Transduction was enriched in clusters 2-5, suggesting increased extracellular communications across differentiation states. Cluster 6 (Fig. 3J), for genes downregulated in both S2D4 and S2D8, was enriched for Metabolism, Transcription Pathway, and, unexpectedly, Neuronal System. Together, transcriptomic analyses supported a global reduction in cell division, transcription, and translation, and a global increase in extracellular communication and inflammation. However, while pathways regulating neurite outgrowth and cytoskeleton reorganization were induced in earlier stages (clusters 2, 3), long-term differentiated cells did not appear to acquire a neuronal fate (cluster 6).

PP121/bufalin leads to a collapse of ADRN CRC and a gain of MES CRC

Considering the upregulation of MES-associated TF PRRX1 in S1D4 and the downregulation of ADRN-associated PHOX2B in S2D4 and S2D30, we visualized additional previously identified TFs associated with MES or ADRN transcriptional programs (*5*). A majority of ADRN TFs appeared to be steadily downregulated over time (Fig. 4A). Interestingly, MES TFs appeared to be upregulated in waves, with a specific subgroup of genes upregulated at a particular stage (Fig. 4B). Next, we combined our data (N=16) with two published neuroblastoma datasets (N=67) (*4*, *35*) and performed gene signature analysis as previously described (*5*). As expected, MES cell lines had high MES scores and low ADRN scores and closely resembled neural crest cells, whereas ADRN cell lines had low MES scores and high ADRN scores (Fig. 4C). Naive SK-N-AS cells exhibited intermediate ADRN-MES state (*4*) and became progressively more MES-like and less ADRN-like at differentiation (Fig. 4C). Additional analyses also showed that differentiated SK-N-AS cells became more immune-activated, which agreed with a recent finding that MES cell lines showed increased immune activation (*36*). We further replicated the positive correlation between MES score and immune activation score (Supp. Fig. 4A), and found a novel positive correlation between MES and senescence scores (*37*) (Supp. Fig. 4A).

To validate RNA-seq analyses at the protein level, we performed IF for naïve and S2D14 cells with antibodies for ADRN-associated TFs PRRX1 and FOSL2 (Fig. 4D). As an ADRN-MES intermediate cell lines, 9.2% and 47% of naïve SK-N-AS cells' nuclei were positive for PRRX1 and FOSL2, respectively, which increased to 45% and 90% in S2D14 cells (Fig. 4E-F). Western blot of naïve and differentiated SK-N-AS cells also showed a complete loss of ADRN-associated TFs PHOX2B and GATA3 starting at S2D7 and a steady increase in FOSL2 starting at S1D4 (Fig.

4G). Therefore, differentiated SK-N-AS cells also showed a gain in MES-associated TFs and a loss of ADRN-associated TFs at the protein levels in agreement with our RNA-seq data.

PP121/bufalin upregulates transcription factors associated with SCPs and chromaffin cells

Various studies have established core regulatory circuits (CRCs) that define the identity of neuroblastoma cells. A new retino-sympathetic CRC was identified in neuroblastoma cells differentiated by RA (*25*). To determine if our PP121/ bufalin-differentiated SK-N-AS cells resembled RA-differentiated neuroblastoma cells, we compared Reactome pathways enriched in down- or -upregulated genes in our cells (S2D30 vs. naive) with neuroblastoma cell lines treated with RA (*25*). There was a significant overlap in pathways of genes downregulated by ATRA and by PP121/ bufalin-differentiated SK-N-AS cells, primarily pathways associated with cell division (Fig. 5A, Supp. Fig. 4B). However, there was much less overlap in the pathways of upregulated genes (Fig. 5B, Supp. Fig. 4C). TFs associated with the retino-sympathetic CRC previously established (*25*) were also downregulated or unchanged, further supporting that PP121/bufalin-induced differentiation was distinct from RA-induced differentiation (Fig. 5C). Remarkably, TFs driving transcriptional programs in chromaffin cells during development (*26*) were upregulated by our differentiation protocol (Fig. 5D). Therefore, we utilized the single-cell RNA database of human neural crest development (*26*) to generate a reference matrix (Supp. Table 4) and deconvolute our RNA-seq using Cibersort (*38*). Naïve SK-N-AS cells were predicted to contain a mix of cycling neuroblasts, chromaffin cells, Schwann cell precursors (SCP), and bridge cells. Over the course of differentiation, the percentage of cycling neuroblast cells decreased, whereas the percentage of chromaffin and SCPs increased (Fig. 5E). However, at the RNA level, while some markers of mature chromaffin and SCP cells increased in S1D4 and S2D4, the majority decreased in S2D30 (Supp Fig. 4D,E), suggesting that these cells resembled intermediate forms of chromaffin cells and SCPs.

PP121/ bufalin promotes long-term differentiation across multiple cell lines

Our data suggested that PP121 completely killed ADRN-type cells but differentiated MES/mix SK-N-AS cells. We further observed that the switch to neurobasal was not necessary for differentiation. Instead, SK-N-AS cells can be differentiated in one step by adding 5 µM PP121 and 10 nM bufalin directly to the growth medium (Fig. 6A). Applying this 1-step protocol, we promoted long-term differentiation of additional MES-type neuroblastoma GIMEN and SHEP cells with 2.5 µM PP121 and 10 nM bufalin (Fig. 6B, Supp Fig. 5A-C, supplementary video) for up to 16 weeks. As previously observed, the addition of PP121 killed ADRN-type SK-N-SH, Kelly, and SH-SY-5Y cells (Supp Fig. 5D-F, supplementary video). Using a similar protocol, we also differentiated and maintained glioblastoma U-251 and LN-229 cells with 5 µM PP121 and 30 nM bufalin (Fig. 6B, supplementary video) for 16 weeks. While the cells did not clump extentsively without bufalin in DMEM or RPMI medium, bufalin further improved long-term cell health for GIMEN and SHEP cells. Interestingly, bufalin was necessary to completely inhibit the proliferation in LN-229 and U-251 cells (Supp Fig. 5G-H). Day 14 (D14) differentiated GIMEN cells showed a loss of MKI67 staining, narrow cell bodies, and a more elaborated network of neurite-like processes (Fig. 6C, E). D14 differentiated SHEP cells also showed a loss of MKI67 and more elongated shapes but not distinct processes (Fig. 6D, F). Similar to SK-N-AS cells,

deconvolution of RNA-seq data from naive and D30 GIMEN cells showed a loss of cycling neuroblasts and cycling SCPs and a gain of chromaffin cells and SCPs (Fig. 6G).

DISCUSSION

Here, we presented a novel strategy for inducing and maintaining the differentiation of SK-N-AS cells over prolonged periods by harnessing the synergistic effects of two compounds - PP121 and bufalin. PP121 functioned to arrest cell proliferation and facilitated the sprouting of cellular processes, while bufalin, a cardiac glycoside, prevented cell clumping and promoted sustained cell health. PP121 and bufalin also differentiated other MES neuroblastoma cells, including GIMEN and SH-EP cells, and glioblastoma cells, including U-251 and LN-229 cells. The drug combination not only triggered cellular differentiation but also preserved the specialized phenotype for an extended duration, with cells maintaining their distinctive characteristics for 16 weeks or more. Notably, various evidence supports that PP121/bufalin-differentiated MES neuroblastoma cells partially resembled chromaffin cells and SCPs, which were distinct from the late neuroblast subtype promoted by RA (*26*). The method's simplicity and versatility present a promising pathway for future research and potential clinical application for high-risk, MES-type neuroblastoma that exhibits resistance to conventional treatment modalities. The long-lived cells generated can also serve as valuable models for studying various processes such as differentiation, maturation, inflammation, senescence, and more.

Although the observed morphological changes are striking and consistent across cell lines, the underlying mechanisms remain unknown. We propose three complementary mechanisms driving cell differentiation (Figg. 7). First, our starting hypothesis is that PP121 induces differentiation by upregulating miR-124. Indeed, miR-124 was permanently upregulated in differentiated SK-N-AS and GIMEN cells (Supp. Fig. 5A, C). Notable miR-124 direct targets that were downregulated in differentiated cells include members of the CDK family regulating cell divisions (*39, 40*) and EZH2 (*41*) and PHF19 (*42*), which are components of the Polycomb Repressive Complex 2 (PRC2) (Supp. Fig. 5B, D). Second, PP121, a dual inhibitor targeting tyrosine kinases and phosphoinositide kinases (*24*), and bufalin, a Na+/K+ ATPase inhibitor (*43*), may induce differentiation through their established mechanisms of action. To test this hypothesis, we compared our RNA-seq results with the Library of Integrated Network-based Cellular Signatures (LINCS) (*44*) using Enrichr (*45*). Interestingly, cluster 1 of SK-N-AS cells and genes upregulated in naïve GIMEN cells (Supp. Fig. 5E, G) were significantly enriched for genes downregulated by Palbociclib, a CDK4/6 inhibitor recently shown to promote the differentiation of ADRN cells (*46*). Genes upregulated in SK-N-AS S2D4, S2D30, and differentiated GIMEN cells, in which bufalin was added, showed a general enrichment for bufalin and other cardiac glycosides and for PI3K inhibitors (Supp. Fig. 5F, H). These results suggested that the known mechanisms of PP121 and bufalin drive parts of the changes in gene expressions observed. Third, epigenetic modifications, both miR-124-dependent and independent, likely play a significant role in cell differentiation. Differentiation of ADRN-type cells by RA involved epigenetic reprogramming (*25*), and miR-124, particularly, is known to drive neuronal differentiation through epigenetic mechanisms (*47*). We also observed an elongation of nuclei in differentiated cells as measured by increased nuclei eccentricity (Supp. Fig. 7), which may suggest chromatin remodeling. Therefore, we propose a

possible synthesis of these pathways in Fig. 7. While further investigation is required to explore these hypotheses, unraveling the complex mechanisms thoroughly will provide valuable insights into neuroblastoma and glioblastoma cell fate decisions and novel therapeutic strategies targeting these cancers.

One significant limitation of our study is the inability of bulk RNA-seq of pooled cell populations (*48*) to fully capture the heterogeneity of the neuroblastoma cell population, particularly evident in SK-N-AS cells, which comprise a mixture of ADRN and MES-type cells. Notably, time-lapse videos revealed diverse cellular morphologies in differentiated SK-N-AS cells, while differentiated GIMEN and SH-EP cells, being predominantly MES-type, appeared more homogeneous. Overcoming these limitations through single-cell analysis is important for comprehending the dynamic processes underlying neuroblastoma progression and differentiation. Future directions also entail a thorough exploration of the mechanisms driving cell differentiation. Furthermore, several studies have supported that cardiac glycosides, including bufalin, are potent anti-cancer compounds (*43*, *49*) but are toxic at high doses (*50*). While *in vivo* data for the efficacy of PP121 is relatively sparse, it was shown to reduce tumor growth in prostate (*51*), thyroid (*52*), and esophageal (*53*) in mouse cancer models. To our knowledge, a combination of PP121/bufalin has not been tested in animal models, which will be necessary to validate observed effects and contextualize therapeutic potential. By leveraging mechanistic insights and preclinical testing, PP121/bufalin-induced differentiation can be potentially developed to inhibit the growth of neural cancers while minimizing toxicity, especially in pediatric patients (*54*), thereby mitigating long-term side effects associated with conventional treatments (*55*).

In conclusion, our innovative protocol offers a promising avenue for treating therapy-resistant neuroblastoma. The long-lived, differentiated cells can be valuable tools for investigating various cellular processes. Therefore, our findings contribute to advancing both basic scientific knowledge and clinical interventions.

ACKNOWLEDGMENT

Funding sources

AMK was funded by the Rainwater Charitable Foundation and NIH NCI 1R01-CA215072.

REG was funded by the NIH R01-CA271605.

SS was funded by a research grant from the Friends of Dana-Farber Cancer Institute.

Author contributions

LDN, SS, and AMK conceived and designed the study.

LDN, SS, KC, and AF performed experiments and analysis for this study.

REG and AMK provided the resources needed for experiments.

LDN wrote an original draft of the manuscript.

LDN, SS, KC, and AMK reviewed and edited the manuscript.

All authors reviewed and commented on the manuscript.

Potential conflict of interests

The authors have no conflicts of interest to declare.

Data and Material Availability

mRNA-sequencing data that support the findings of this study will be deposited into the Gene Expression Omnibus (GEO) Repository. CPM numbers are provided in supp. Table 8. Contact the corresponding author to request materials and cell lines used in the manuscript.

MATERIALS AND METHODS

Immortalized and Primary Rat Cortical Neuron Culture

SK-N-AS, SK-N-SH, SH-SY-5Y, Kelly, LN-229, and U-251 cells were maintained in DMEM+ GlutaMAX™ supplemented with 10% fetal bovine serum (FBS) and 1% penicillin/streptomycin (P/S). GIMEN and SH-EP were maintained in RPMI 1640 Medium + GlutaMAX™ supplemented with 10% FBS and 1% penicillin/streptomycin (P/S). Cells were cultured in a standard incubator set to a controlled environment of 5% CO_2 and 37°C and checked for mycoplasma contamination every 3 months.

The protocol for primary rat neuron preparation was approved by the Institutional Animal Care and Use Committee at Brigham and Women's Hospital. Rat primary cortical neuron cultures were prepared from E18 SAS Sprague Dawley pups (Charles River). Brain tissues were dissected, dissociated enzymatically by 0.25% Trypsin-EDTA (Thermo Fisher Scientific), triturated with fire-polished glass Pasteur pipettes, and passed through a 40 µm cell strainer (Sigma-Aldrich). After counting, neurons were seeded onto poly-D-lysine (Sigma-Aldrich) coated cell culture plates at 80,000 cells/cm2 in Neurobasal medium supplemented with 1X B27 and 0.25X GlutaMax. Half medium was changed every 4 days until use.

miR-124 Transfection

miR-124 mimics or non-targeted CTRL (Horizon Discovery) were dissolved in water to 50 µM concentration and used at the final concentration of 50 nM. Transfection into cultured SK-N-AS cells was performed using Lipofectamine 2000 (Thermo Fisher Scientific) following standard protocols. After a 24-hour incubation period, the transfection medium was replaced with a fresh growth medium, and cells were subsequently analyzed for confluence and viability 4 days after transfection.

Incucyte Live Imaging

Live cell imaging was performed using the IncuCyte™ Live-Cell Imaging System (Sartorius) at 20X magnification. Cell confluence was quantified using the IncuCyte™ software.

WST-1 Cell Viability Assay

Cell viability was measured by WST-1 reduction assay (Sigma-Aldrich). For the assay, all medium was removed and replaced with 1X WST-1 reagent dissolved in the growth medium, followed by 1 hour of incubation at 37°C. The absorbance of the culture medium was measured with a microplate reader at test and reference wavelengths of 450 nm and 630 nm, respectively.

Drug Treatment

PP121 (Medchemexpress) was dissolved to 10 mM in DMSO and used at final concentrations of 2.5 – 10 µM. Bufalin (Fisher Scientific) was dissolved to 1 mM in DMSO and used at final concentrations of 10 – 100 nM. Detailed concentrations used to differentiate each cell line were listed in supp. Table 5.

RNA Collection and RT-qPCR

Total RNA from cells was extracted using the Norgen Total RNA Purification Kit (Norgen Biotek) following the manufacturer's protocol. DNAse1 was applied during RNA extraction to remove genomic DNA. RNA was eluted in nuclease-free water, and the concentration was measured using Nanodrop (Thermo Fisher Scientific). For miRNA analysis, 50ng of RNA was reverse transcribed into cDNA using the miRCURY LNA RT kit (Qiagen). RT-qPCR mix was prepared using the miRCURY LNA SYBR Green PCR kit (Qiagen). qPCR was performed using the QuantStudio 7 Flex System. The cycling conditions were 95°C for 10 min, 50 cycles of 95°C for 15 s, and 60°C for 1 min following dissociation analysis. miRNA expression was normalized let-7a.

Quantification was performed using the delta-delta Ct method. miRNA and mRNA primers used were listed in Supp. Table 6.

Immunofluorescent Staining and Analysis

Cells plated on coverslips were fixed with 4% (v/v) formaldehyde-PBS for 15 min, washed in PBS (Corning), incubated in 1X blocking/permeabilization buffer (Biotium) for 1h, and incubated with primary antibodies overnight at 1:100 dilution. Coverlips were washed with PBS and incubated with the corresponding AlexaFluor-conjugated secondary antibodies at 1:500 dilution (Life Technologies) for 2h at room temperature. After washing, coverslips were mounted onto glass slides containing DAPI mounting medium. Image acquisition was done with a Zeiss LSM 710 Confocal Microscope. Primary and secondary antibodies used were listed in Supp. Tables 7. MKI67 expression and morphology analyses were conducted with CellProfiler software (*56*). Custom pipelines were developed for each cell line, with the same pipeline used for naïve and differentiated cells of the same line.

RNA-seq and Transcriptomic analyses

After quality control by Agilent 2100 Bioanalyzer, the total RNA was used as input for library preparation by Novogene Co., Ltd, followed by high-throughput sequencing on Illumina HiSeq X with PE150 mode to produce approximately 20 M reads per sample. Raw data alignment and differential gene expression analysis were performed using the BioJupies web application (*57*).For heatmap and k-means clustering, the CPM values were first normalized internally for each gene. Python's scikit-learn library was used to perform k-mean clustering into 6 clusters. Gene ontology analyses were performed using Enrichr (*45*)

Gene Signature Analysis

Gene signature analysis utilized gene lists identified in previous studies: MES-specific and ADRN-specific genes (*5*), immune activation genes (*36*), and senescence genes (*37*). Genes were rank-ordered according to their CPM level, and the percentile was calculated relative to the full list. For each gene set, the percentile averages were Z-transformed across samples and then used as a signature score.

Western Blots

Total protein was extracted using RIPA buffer (Boston Bioproducts) supplemented with Complete, Mini, EDTA-free Protease Inhibitor Cocktail (Millipore Sigma). Protein concentrations were determined using the Micro BCA Protein Assay Kit (Thermo Fisher Scientific). Equal amounts of protein were loaded, and electrophoresis was performed in NuPAGE 4 to 12% gradient Bis-Tris polyacrylamide protein gels (Thermo Fisher Scientific). Proteins were transferred to Immun-Blot PVDF membranes (Bio-Rad) and then blocked with 5% milk in tris-buffered saline with 0.1% Tween (TBS-T, Boston Bioproduct) for 1 h. Membranes were incubated overnight with primary antibodies at 4 °C. Blots were washed and incubated with secondary antibodies for 2 h at room temperature. After washing, bands were visualized with ECL chemiluminescence reagents (Genesee Scientific) using the iBright Imaging System (Thermo Fisher Scientific). Band intensity

was measured using the Image Studio Lite software (LI-COR Biosciences). Antibodies and other key resources are listed in Supp. Tables 7.

Deconvolution of Bulk RNA-seq

Single-cell RNA-seq data from the developing human adrenal gland was downloaded (*26*) and used to prepare the reference matrix with the CIBERSORTx web application (*38*). This reference matrix was then used to deconvolute bulk RNA-seq data with CIBERSORTx.

Statistical Analysis

Data management and calculations were performed using Prism 10 (GraphPad). Comparisons between two groups were done using the unpaired two-tailed Student's t-test. A P value < 0.05 was considered statistically significant, and the following notations are used in all figures: $*P < 0.05$, $**P < 0.01$, $***P < 0.001$, and $****P < 0.0001$. All error bars shown represent mean +/− standard deviation (SD) unless otherwise stated.

REFERENCES

1. S. B. Whittle *et al.*, Overview and recent advances in the treatment of neuroblastoma. *Expert Rev Anticancer Ther* **17**, 369-386 (2017).
2. R. A. Ross, B. A. Spengler, J. L. Biedler, Coordinate morphological and biochemical interconversion of human neuroblastoma cells. *J Natl Cancer Inst* **71**, 741-747 (1983).
3. W. J. Rettig, B. A. Spengler, P. G. Chesa, L. J. Old, J. L. Biedler, Coordinate changes in neuronal phenotype and surface antigen expression in human neuroblastoma cell variants. *Cancer Res* **47**, 1383-1389 (1987).
4. V. Boeva *et al.*, Heterogeneity of neuroblastoma cell identity defined by transcriptional circuitries. *Nat Genet* **49**, 1408-1413 (2017).
5. T. van Groningen *et al.*, Neuroblastoma is composed of two super-enhancer-associated differentiation states. *Nat Genet* **49**, 1261-1266 (2017).
6. T. van Groningen *et al.*, A NOTCH feed-forward loop drives reprogramming from adrenergic to mesenchymal state in neuroblastoma. *Nat Commun* **10**, 1530 (2019).
7. L. Wang *et al.*, ASCL1 characterizes adrenergic neuroblastoma via its pioneer function and cooperation with core regulatory circuit factors. *Cell Rep* **42**, 113541 (2023).
8. E. M. Westerhout *et al.*, Mesenchymal-Type Neuroblastoma Cells Escape ALK Inhibitors. *Cancer Res* **82**, 484-496 (2022).
9. N. W. Mabe *et al.*, Transition to a mesenchymal state in neuroblastoma confers resistance to anti-GD2 antibody via reduced expression of ST8SIA1. *Nat Cancer* **3**, 976-993 (2022).
10. N. A. M. Shendy, M. W. Zimmerman, B. J. Abraham, A. D. Durbin, Intrinsic transcriptional heterogeneity in neuroblastoma guides mechanistic and therapeutic insights. *Cell Rep Med* **3**, 100632 (2022).
11. H. Galagali, J. K. Kim, The multifaceted roles of microRNAs in differentiation. *Curr Opin Cell Biol* **67**, 118-140 (2020).
12. E. V. Makeyev, J. Zhang, M. A. Carrasco, T. Maniatis, The MicroRNA miR-124 promotes neuronal differentiation by triggering brain-specific alternative pre-mRNA splicing. *Mol Cell* **27**, 435-448 (2007).
13. A. S. Yoo *et al.*, MicroRNA-mediated conversion of human fibroblasts to neurons. *Nature* **476**, 228-231 (2011).

14. J. Y. Yu, K. H. Chung, M. Deo, R. C. Thompson, D. L. Turner, MicroRNA miR-124 regulates neurite outgrowth during neuronal differentiation. *Exp Cell Res* **314**, 2618-2633 (2008).
15. K. C. Sonntag, T. U. Woo, A. M. Krichevsky, Converging miRNA functions in diverse brain disorders: a case for miR-124 and miR-126. *Exp Neurol* **235**, 427-435 (2012).
16. X. Jia *et al.*, MicroRNA-124: An emerging therapeutic target in cancer. *Cancer Med* **8**, 5638-5650 (2019).
17. L. Lima *et al.*, Modulation of all-trans retinoic acid-induced MiRNA expression in neoplastic cell lines: a systematic review. *BMC Cancer* **19**, 866 (2019).
18. P. Laneve *et al.*, The interplay between microRNAs and the neurotrophin receptor tropomyosin-related kinase C controls proliferation of human neuroblastoma cells. *Proc Natl Acad Sci U S A* **104**, 7957-7962 (2007).
19. N. J. Beveridge, P. A. Tooney, A. P. Carroll, N. Tran, M. J. Cairns, Down-regulation of miR-17 family expression in response to retinoic acid induced neuronal differentiation. *Cell Signal* **21**, 1837-1845 (2009).
20. E. Das, N. P. Bhattacharyya, MicroRNA-432 contributes to dopamine cocktail and retinoic acid induced differentiation of human neuroblastoma cells by targeting NESTIN and RCOR1 genes. *FEBS Lett* **588**, 1706-1714 (2014).
21. L. Samaraweera, K. B. Grandinetti, R. Huang, B. A. Spengler, R. A. Ross, MicroRNAs define distinct human neuroblastoma cell phenotypes and regulate their differentiation and tumorigenicity. *BMC Cancer* **14**, 309 (2014).
22. L. D. Nguyen *et al.*, Small molecule regulators of microRNAs identified by high-throughput screen coupled with high-throughput sequencing. *Nat Commun* **14**, 7575 (2023).
23. L. D. Nguyen, R. K. Chau, A. M. Krichevsky, Small Molecule Drugs Targeting Non-Coding RNAs as Treatments for Alzheimer's Disease and Related Dementias. *Genes (Basel)* **12**, (2021).
24. B. Apsel *et al.*, Targeted polypharmacology: discovery of dual inhibitors of tyrosine and phosphoinositide kinases. *Nat Chem Biol* **4**, 691-699 (2008).
25. M. W. Zimmerman *et al.*, Retinoic acid rewires the adrenergic core regulatory circuitry of childhood neuroblastoma. *Sci Adv* **7**, eabe0834 (2021).
26. S. Jansky *et al.*, Single-cell transcriptomic analyses provide insights into the developmental origins of neuroblastoma. *Nat Genet* **53**, 683-693 (2021).
27. B. Roy, M. Dunbar, R. C. Shelton, Y. Dwivedi, Identification of MicroRNA-124-3p as a Putative Epigenetic Signature of Major Depressive Disorder. *Neuropsychopharmacology* **42**, 864-875 (2017).
28. A. Voigt, P. Hartmann, F. Zintl, Differentiation, proliferation and adhesion of human neuroblastoma cells after treatment with retinoic acid. *Cell Adhes Commun* **7**, 423-440 (2000).
29. A. Singh *et al.*, Retinoic acid induces REST degradation and neuronal differentiation by modulating the expression of SCF(beta-TRCP) in neuroblastoma cells. *Cancer* **117**, 5189-5202 (2011).
30. M. M. Shipley, C. A. Mangold, M. L. Szpara, Differentiation of the SH-SY5Y Human Neuroblastoma Cell Line. *J Vis Exp*, 53193 (2016).
31. S. Garofalo *et al.*, The Glycoside Oleandrin Reduces Glioma Growth with Direct and Indirect Effects on Tumor Cells. *J Neurosci* **37**, 3926-3939 (2017).
32. R. L. Gomez *et al.*, Super-enhancer associated core regulatory circuits mediate susceptibility to retinoic acid in neuroblastoma cells. *Front Cell Dev Biol* **10**, 943924 (2022).

33. J. D. Whittard, T. Sakurai, M. R. Cassella, M. Gazdoiu, D. P. Felsenfeld, MAP kinase pathway-dependent phosphorylation of the L1-CAM ankyrin binding site regulates neuronal growth. *Mol Biol Cell* **17**, 2696-2706 (2006).
34. R. G. Hodge, A. J. Ridley, Regulating Rho GTPases and their regulators. *Nat Rev Mol Cell Biol* **17**, 496-510 (2016).
35. J. L. Harenza *et al.*, Transcriptomic profiling of 39 commonly-used neuroblastoma cell lines. *Sci Data* **4**, 170033 (2017).
36. S. Sengupta *et al.*, Mesenchymal and adrenergic cell lineage states in neuroblastoma possess distinct immunogenic phenotypes. *Nat Cancer* **3**, 1228-1246 (2022).
37. D. Saul *et al.*, A new gene set identifies senescent cells and predicts senescence-associated pathways across tissues. *Nat Commun* **13**, 4827 (2022).
38. A. M. Newman *et al.*, Robust enumeration of cell subsets from tissue expression profiles. *Nat Methods* **12**, 453-457 (2015).
39. J. Silber *et al.*, Expression of miR-124 inhibits growth of medulloblastoma cells. *Neuro Oncol* **15**, 83-90 (2013).
40. T. Feng *et al.*, MiR-124 inhibits cell proliferation in breast cancer through downregulation of CDK4. *Tumour Biol* **36**, 5987-5997 (2015).
41. W. H. Neo *et al.*, MicroRNA miR-124 controls the choice between neuronal and astrocyte differentiation by fine-tuning Ezh2 expression. *J Biol Chem* **289**, 20788-20801 (2014).
42. J. Lu, H. Ji, H. Tang, Z. Xu, microRNA-124a suppresses PHF19 over-expression, EZH2 hyper-activation, and aberrant cell proliferation in human glioma. *Biochem Biophys Res Commun* **503**, 1610-1617 (2018).
43. I. Prassas, E. P. Diamandis, Novel therapeutic applications of cardiac glycosides. *Nat Rev Drug Discov* **7**, 926-935 (2008).
44. A. B. Keenan *et al.*, The Library of Integrated Network-Based Cellular Signatures NIH Program: System-Level Cataloging of Human Cells Response to Perturbations. *Cell Syst* **6**, 13-24 (2018).
45. Z. Xie *et al.*, Gene Set Knowledge Discovery with Enrichr. *Curr Protoc* **1**, e90 (2021).
46. K. M. Ferguson *et al.*, Palbociclib releases the latent differentiation capacity of neuroblastoma cells. *Dev Cell* **58**, 1967-1982 e1968 (2023).
47. D. G. Abernathy *et al.*, MicroRNAs Induce a Permissive Chromatin Environment that Enables Neuronal Subtype-Specific Reprogramming of Adult Human Fibroblasts. *Cell Stem Cell* **21**, 332-348 e339 (2017).
48. A. S. Thind *et al.*, Demystifying emerging bulk RNA-Seq applications: the application and utility of bioinformatic methodology. *Brief Bioinform* **22**, (2021).
49. X. Sun *et al.*, Bufalin, a Traditional Chinese Medicine Compound, Prevents Tumor Formation in Two Murine Models of Colorectal Cancer. *Cancer Prev Res (Phila)* **12**, 653-666 (2019).
50. S. Kanji, R. D. MacLean, Cardiac glycoside toxicity: more than 200 years and counting. *Crit Care Clin* **28**, 527-535 (2012).
51. T. Bello *et al.*, Computational modeling identifies multitargeted kinase inhibitors as effective therapies for metastatic, castration-resistant prostate cancer. *Proc Natl Acad Sci U S A* **118**, (2021).
52. H. Y. Che, H. Y. Guo, X. W. Si, Q. Y. You, W. Y. Lou, PP121, a dual inhibitor of tyrosine and phosphoinositide kinases, inhibits anaplastic thyroid carcinoma cell proliferation and migration. *Tumour Biol* **35**, 8659-8664 (2014).
53. Y. Peng *et al.*, The anti-esophageal cancer cell activity by a novel tyrosine/phosphoinositide kinase inhibitor PP121. *Biochem Biophys Res Commun* **465**, 137-144 (2015).
54. C. Ikonomidou, Chemotherapy and the pediatric brain. *Mol Cell Pediatr* **5**, 8 (2018).

55. L. D. Nguyen, B. E. Ehrlich, Cellular mechanisms and treatments for chemobrain: insight from aging and neurodegenerative diseases. *EMBO Mol Med* **12**, e12075 (2020).
56. D. R. Stirling *et al.*, CellProfiler 4: improvements in speed, utility and usability. *BMC Bioinformatics* **22**, 433 (2021).
57. D. Torre, A. Lachmann, A. Ma'ayan, BioJupies: Automated Generation of Interactive Notebooks for RNA-Seq Data Analysis in the Cloud. *Cell Syst* **7**, 556-561 e553 (2018).

List of figures, supplementary figures, and supplementary tables

Figures

Figure 1: PP121 upregulates miR-124 and drives differentiation of SK-N-AS cells.

Figure 2: PP121 and bufalin synergistically differentiate SK-N-AS cells over 30 days.

Figure 3: PP121/bufalin drives transcriptional changes associated with non-neuronal differentiation of SK-N-AS cells.

Figure 4: PP121/bufalin leads to a collapse of ADRN CRC and a gain of MES CRC.

Figure 5: Differentiated SK-N-AS cells show a gain in TFs associated with chromaffin and SCP states.

Figure 6: PP121/ Bufalin promotes the differentiation of multiple cell lines.

Figure 7: Proposed mechanisms contributing to PP121/bufalin-induced cellular differentiation.

Supplementary Figures

Supplementary Figure 1: PP121 reversibly differentiates SK-N-AS cells.

Supplementary Figure 2: In combination with PP121, cardiac glycosides prevent clumping and promote neurite-like processes.

Supplementary Figure 3: PP121/bufalin promotes long-term differentiation into heterogeneous cell populations

Supplementary Figure 4: PP121/bufalin-induced differentiation is distinct from RA-induced differentiation.

Supplementary Figure 5: Impact of PP121/bufalin on various cell lines.

Supplementary Figure 6: miR-124 and drug signature in differentiated cells.

Supplementary Figure 7: Differentiation is associated with changes in nuclear morphology.

Supplementary Tables

Supplementary Table 1: List of 22 candidate compounds and their characteristics

Supplementary Table 2: Confluence growth with candidate compound treatment over 4 days

Supplementary Table 3: List of genes in each of the 6 clusters identified and their Z-scores.

Supplementary Table 4: Single-cell reference matrix for the developing adrenal medulla

Supplementary Table 5: Optimized differentiation conditions for various cell lines

Supplementary Table 6: Primers used in this study

Supplementary Table 7: Other key resources used in this study

Supplementary Table 8: Count matrix (CPM) of SK-N-AS and GIMEN cells

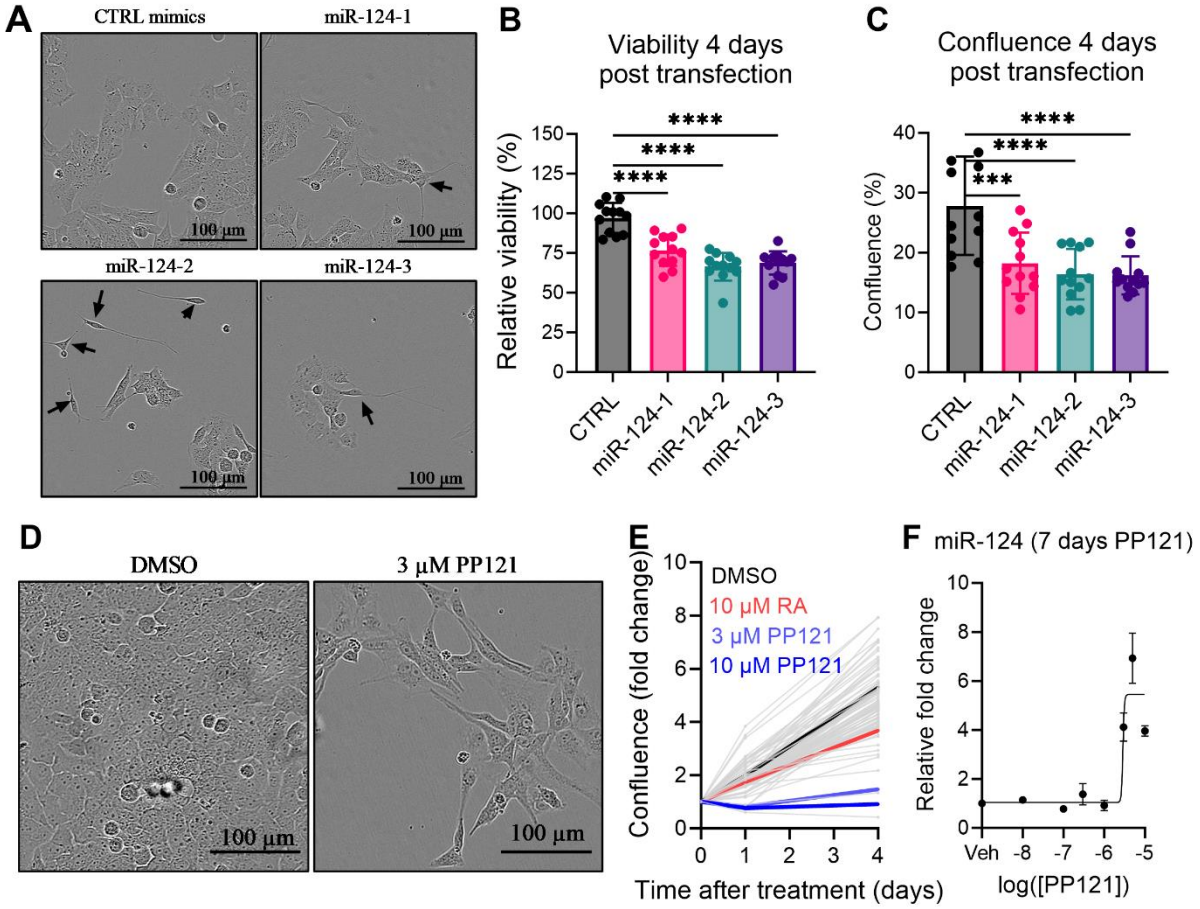

Figure 1: PP121 upregulates miR-124 and drives differentiation of SK-N-AS cells. (A) Transfection of miR-124 mimics transformed some cells (black arrows) into acquiring neuronal morphology, **(B)** decreased cell viability, and **(C)** confluence growth (N=12, 1-way ANOVA, Dunnet's multiple comparisons **(D)** Representative images of SK-N-AS 4 days after treatment with DMSO, 3µM PP121, and 10 µM ATRA. **(E)** Normalized confluence growth over 4 days with treatments (N = 1 per dose per drug, N = 5 for DMSO). **(F)** 5 uM PP121 maximally upregulated miR-124 in SK-N-AS cells 7 days after treatment (N=4-6 per concentration).

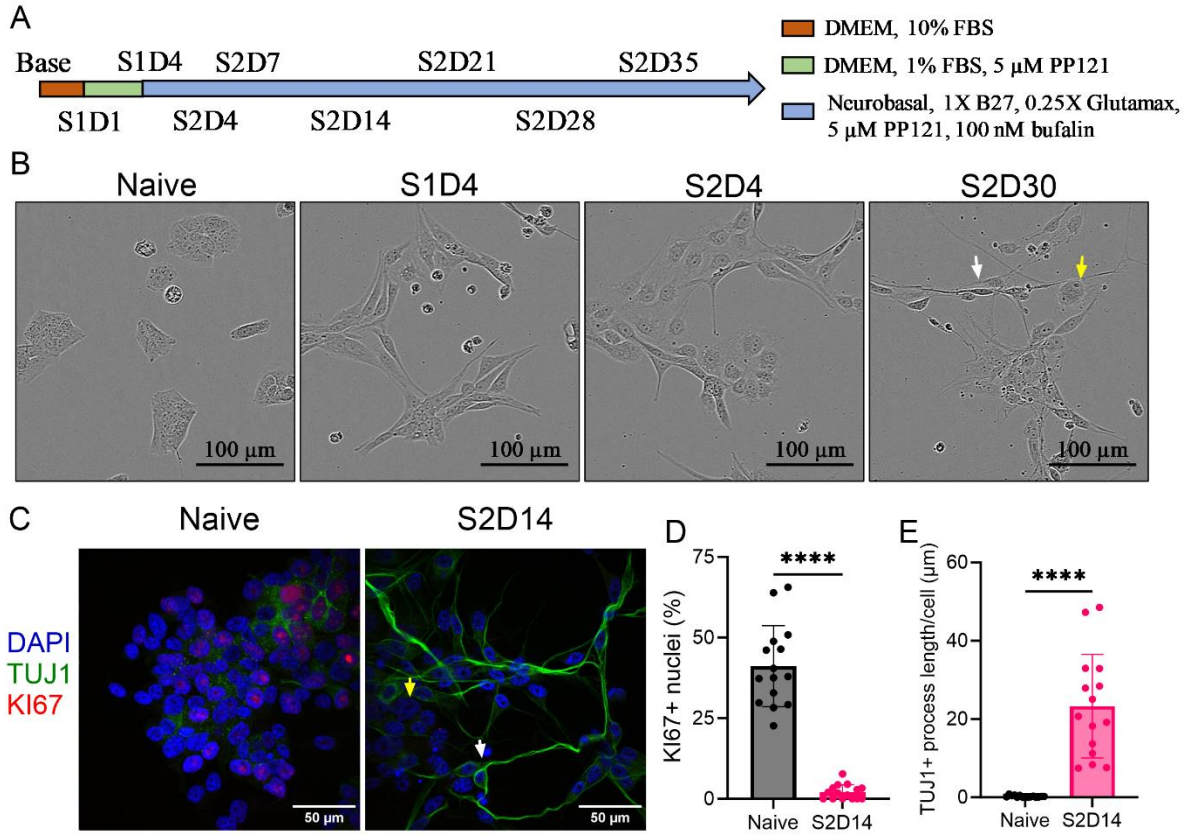

Figure 2: PP121 and bufalin synergistically differentiate SK-N-AS cells (A) Schematic of optimized differentiation protocol for SK-N-AS cells. In stage 2, 20% of medium is added every 7 days to replace the amount evaporated. **(B)** Representative images of cells over 30 days of differentiation. **(C)** Representative immunofluorescent images of naive and S2D14 cells. **(D-E)** Quantification of KI67-positive nuclei and TUJ1-positive processes (n=15 images per group, student t-test). The white arrow pointed to neuron-like cells with small cell bodies and neurite-like processes; the yellow arrow pointed to senescent-like cells with enlarged cell bodies and no processes.

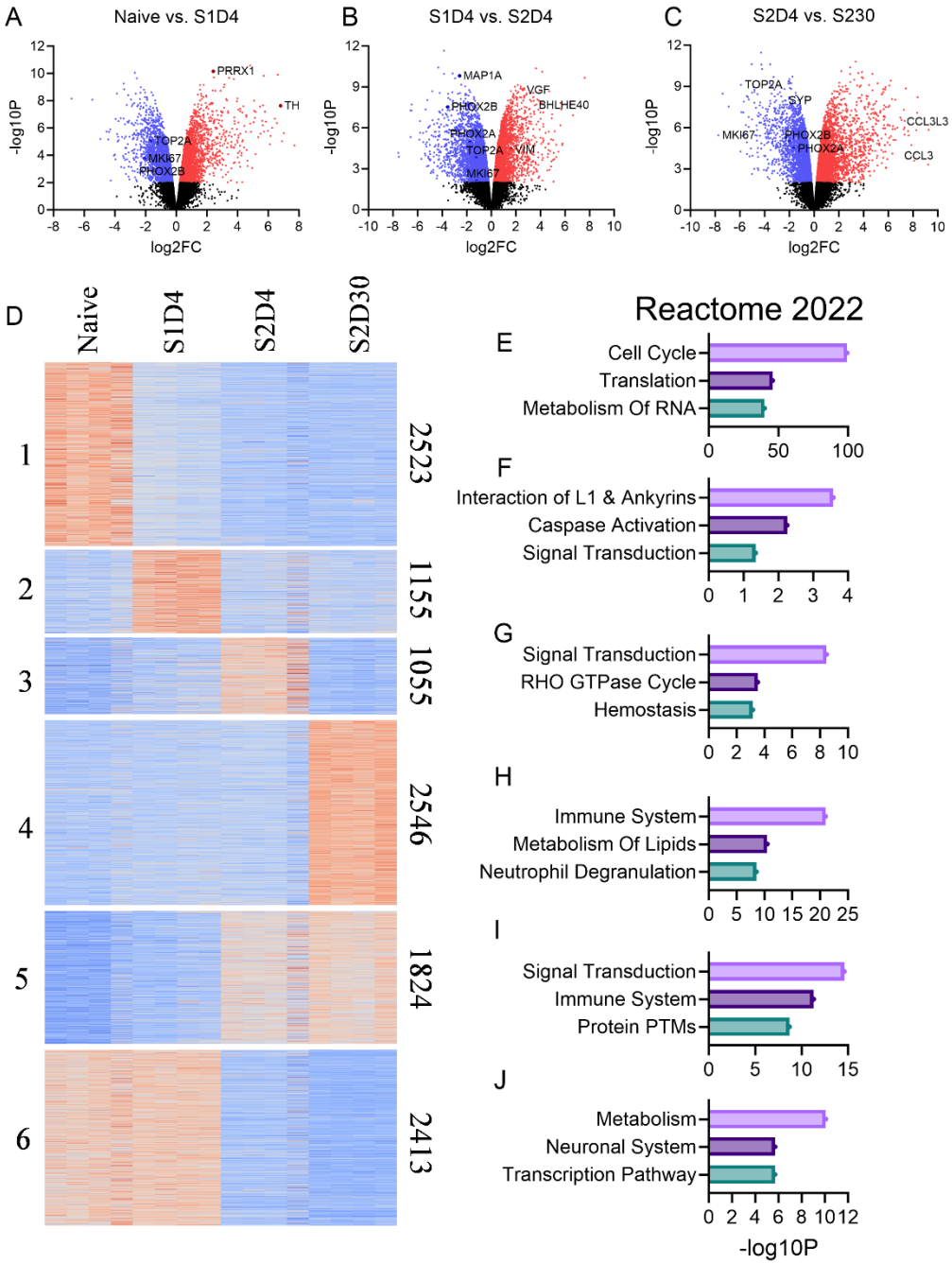

Figure 3: PP121/bufalin drives transcriptional changes associated with non-neuronal differentiation of SK-N-AS cells. (A-C) Volcano plots comparing different stages of SK-N-AS differentiation. Significantly downregulated or upregulated genes were colored blue and red respectively (N=4 per stage). **(D)** Heatmap of all genes differentially expressed across 4 states. Z-score scaling was applied internally for each gene before K-mean clustering. Numbers on the left indicate the cluster, and numbers on the right indicate the number of genes in each cluster. **(E-J)** Top Reactome pathway enrichment analyses for each cluster in D (Table S3 for complete list).

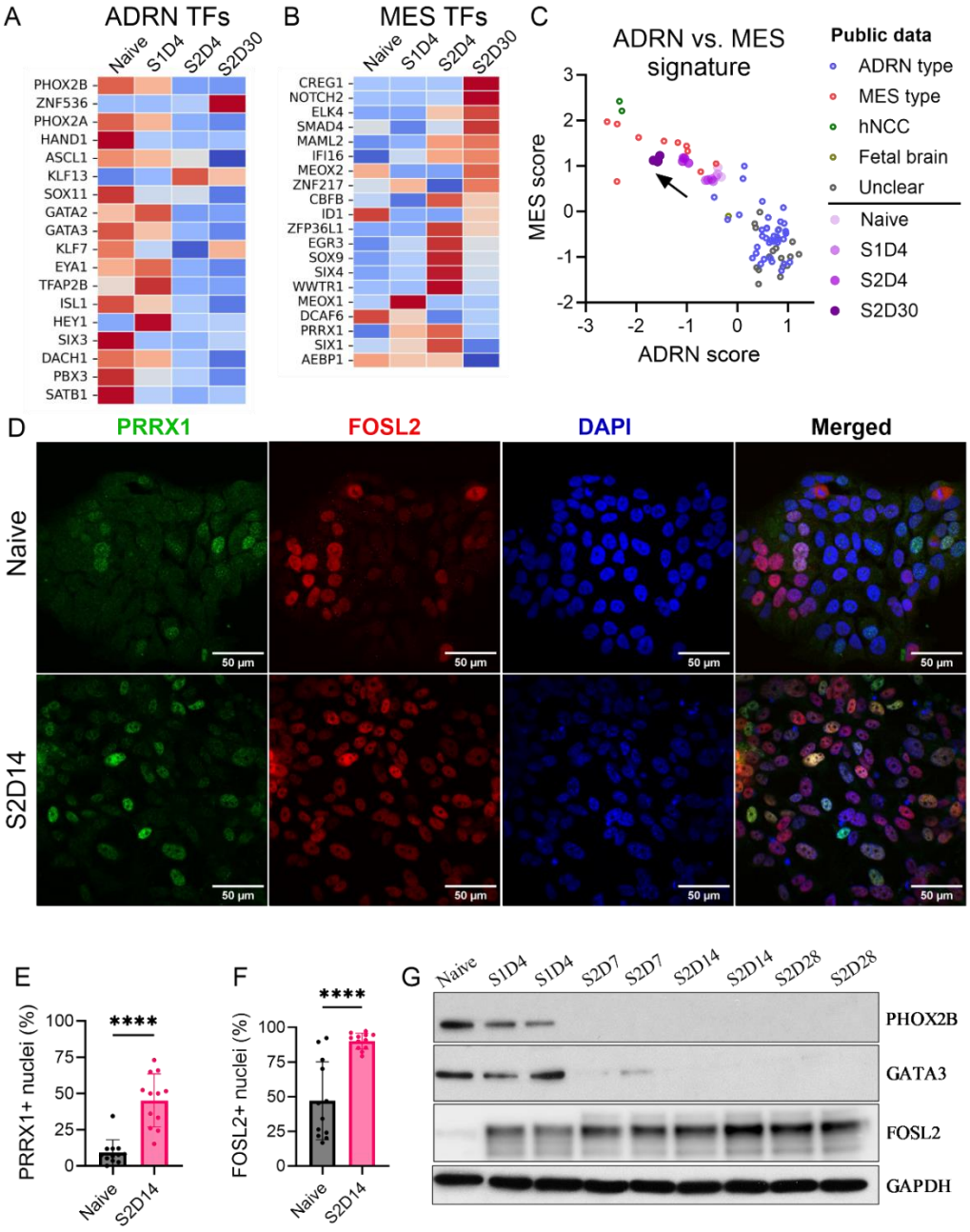

Figure 4: PP121/bufalin leads to a collapse of ADRN CRC and a gain of MES CRC. (A-B) Averaged heatmap (N=4) for ADRN and MES TFs. Z-score scaling was applied internally for each gene. **(C)** Differentiated SK-N-AS cells became increasingly more MES and less ADRN (From public databases, N =67 samples; from this study, N = 16 total, 4 per group). **(D)** Representative IF images for naïve and S2D14 SK-N-AS cells. **(E-F)** Quantification of PRRX1-positive and FOSL2-positive nuclei (n=12 images per group, student t-test). **(G)** Representative Western blot of naïve and differentiated SK-N-AS cells over time.

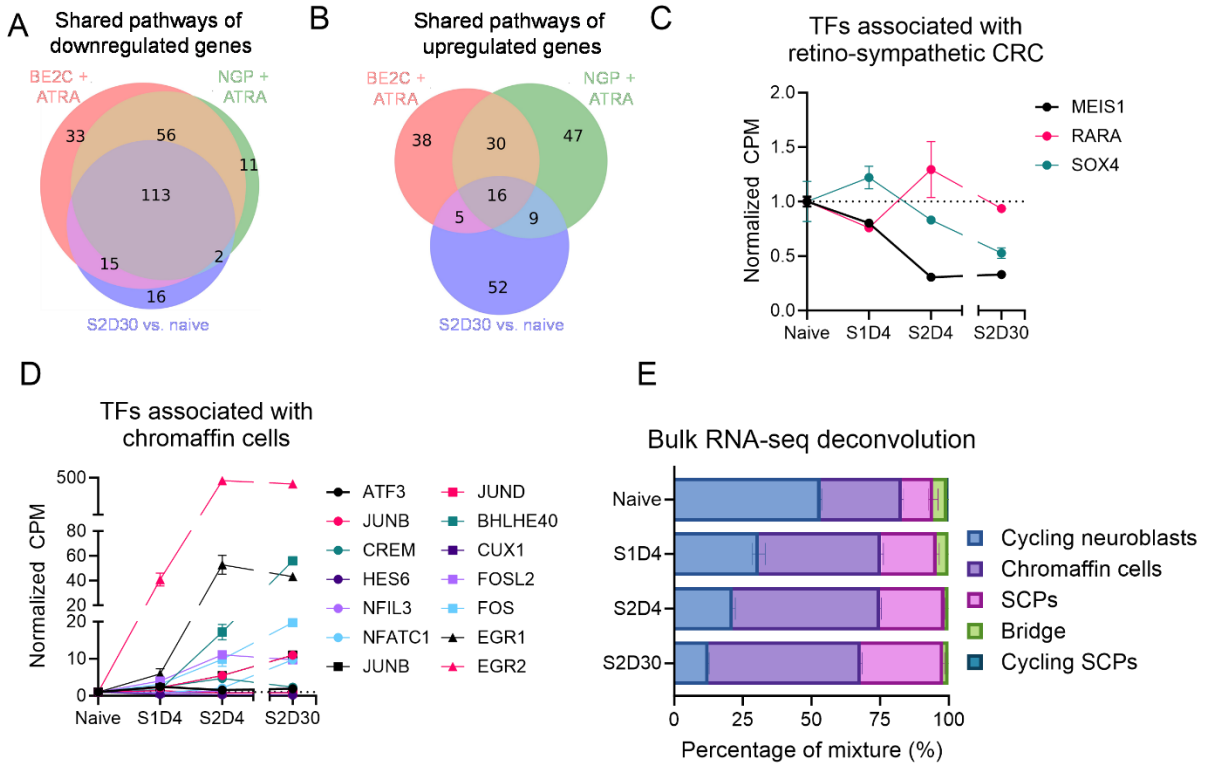

Figure 5: Differentiated SK-N-AS cells show a gain in TFs associated with chromaffin and SCP state. (A-B) Shared down- and up-regulated pathways among SK-N-AS cells differentiated with PP121/ bufalin, and BE2C and NGP cells differentiated with RA. **(C)** TF associated with retino-sympathetic CRC were downregulated or unchanged. **(D)** TFs associated with chromaffin cells were generally upregulated. **(E)** Deconvolution of bulk RNA-seq results of naïve and differentiated SK-N-AS cells (N=4).

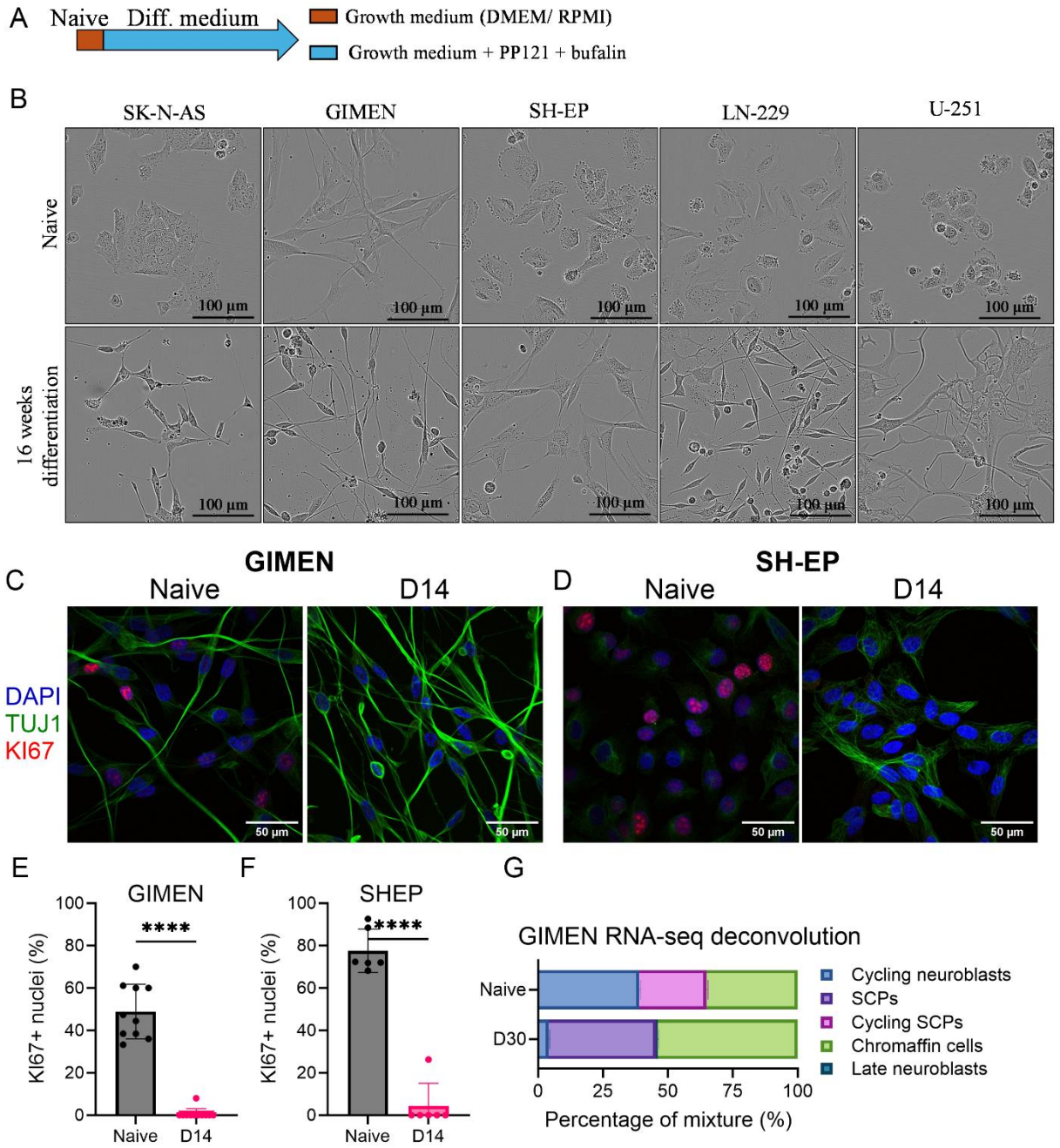

Figure 6: PP121/ Bufalin promotes the differentiation of multiple cell lines. (A) Schematic of 1-step differentiation protocol. **(B)** Representative live cell images of SK-N-AS, GIMEN, SHEP, U-251, and LN-229 after 16 weeks of differentiation. **(C-D)** Representative IF images of naïve and D14 GIMEN and SHEP cells. **(E-F)** Quantification of KI67-positive nuclei in GIMEN (N=12) and SHEP (N=6) cells. **(G)** Deconvolution of bulk RNA-seq results of naïve and D30 differentiated GIMEN cells (N=3).

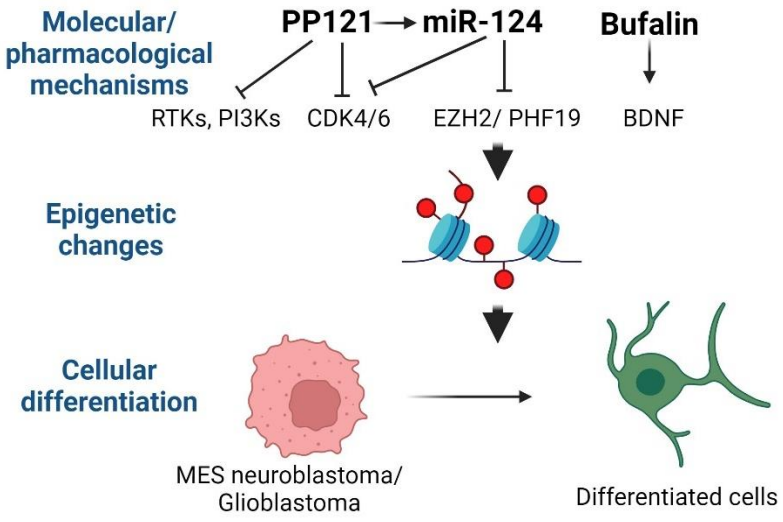

Figure 7: Proposed possible mechanisms for PP121/bufalin-induced differentiation of neuroblastoma and glioblastoma cells.

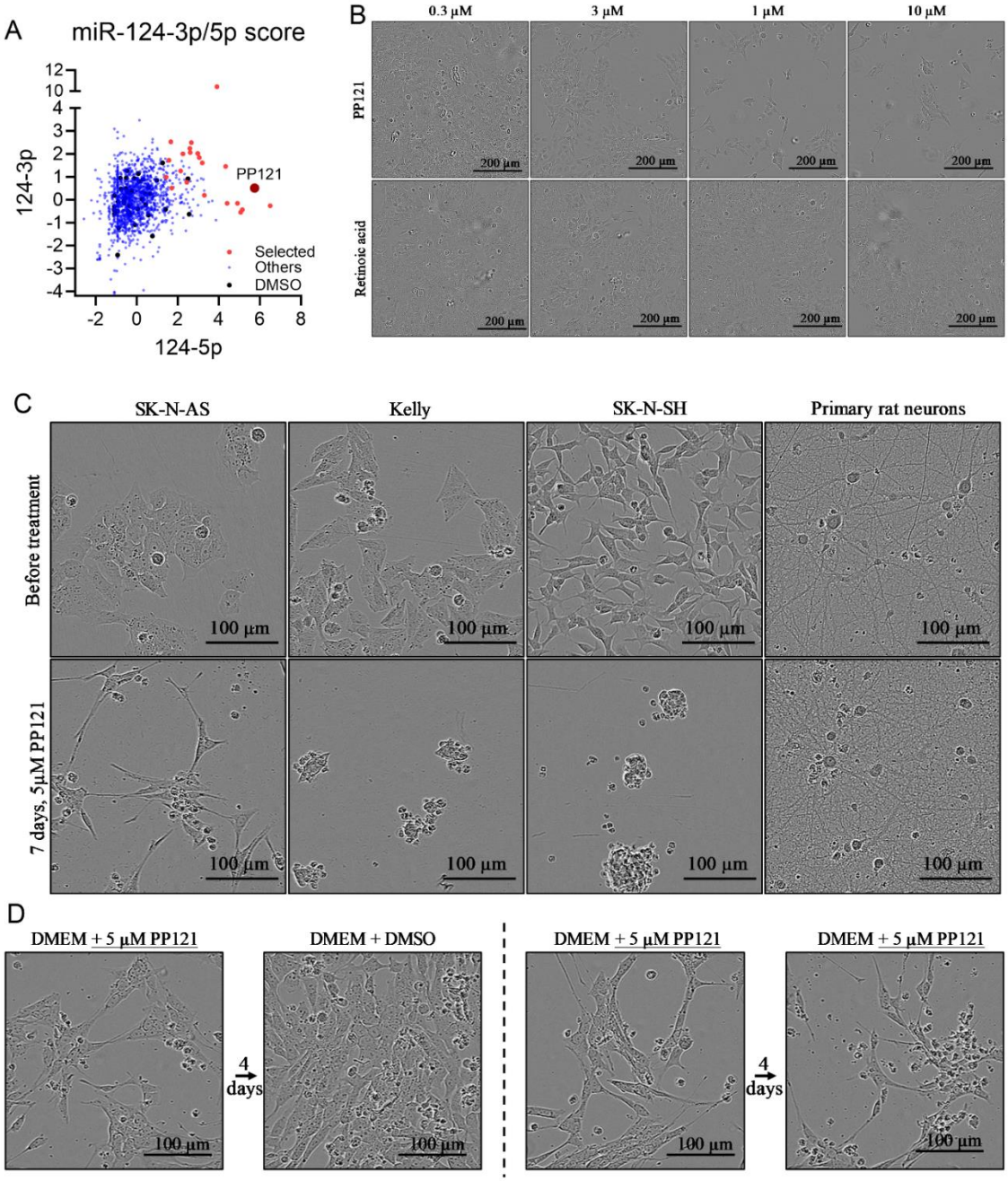

Supplementary Figure 1: PP121 reversibly differentiates SK-N-AS cells. **(A)** Graph showing COMBAT score of all compounds, candidate compounds were shown in red, DMSO controls in black, and other compounds in blue. **(B)** Representative images of SK-N-AS 4 days after treatment with 4 different doses of PP121 and RA. (**C)** Representative images of various cell lines 7 days after treatment with 5μM PP121. (**D)** Representative images of SK-N-AS 4 days after 5 μM PP121, followed by 4 days of fresh medium containing DMSO or 5 μM PP121.

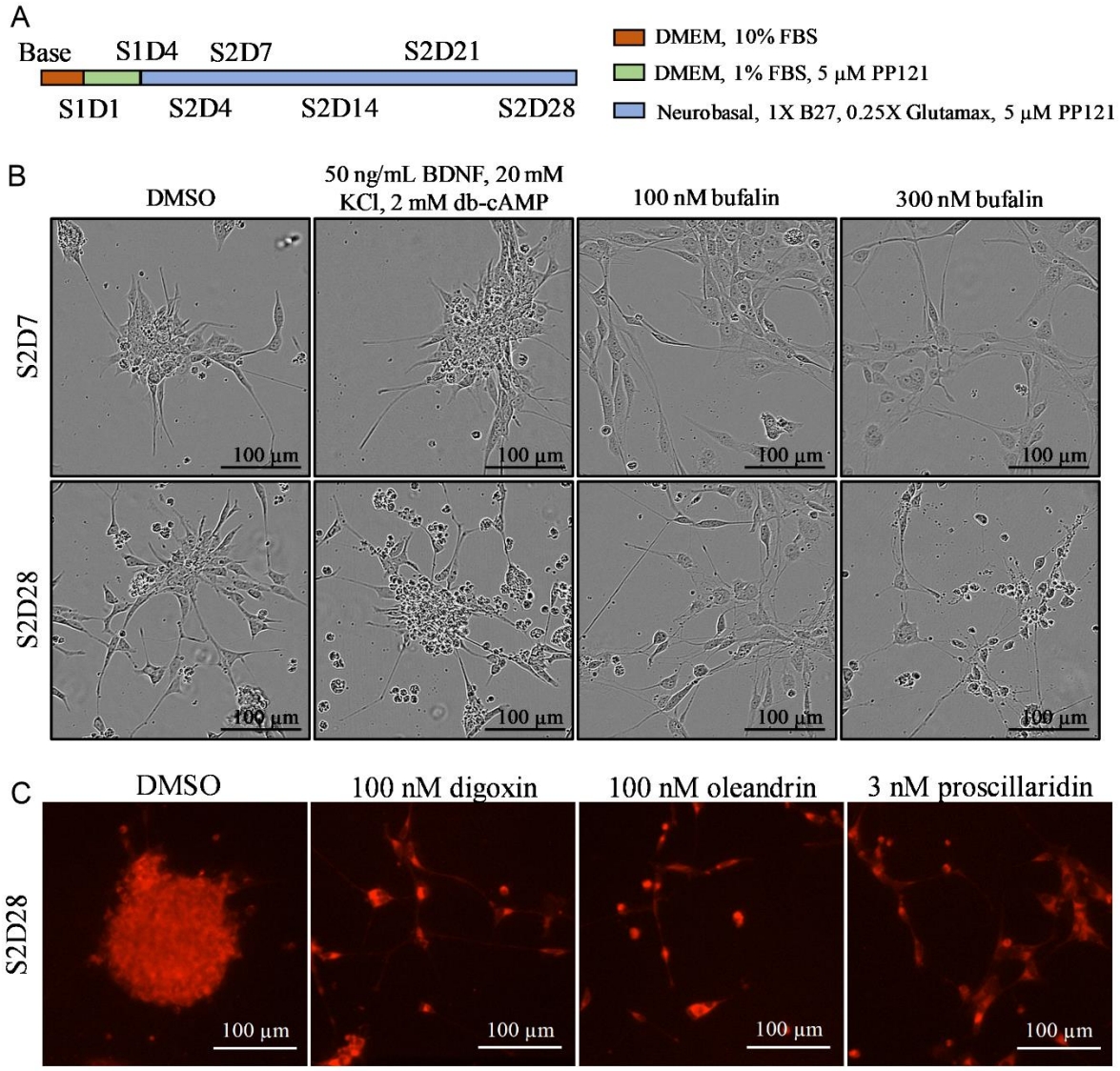

Supplementary Figure 2: In combination with PP121, cardiac glycosides prevent clumping and promote neurite-like processes. (A) Differentiation protocol based on previous protocol to differentiate SH-SY-5Y cells with RA **(B)** Representative images of SK-N-AS in 1 week and 4 weeks in S2 medium with DMSO, BDNF/KCl/db-cAMP, and bufalin **(C)** Representative images of SK-N-AS 28 stained with a membrane TRITC dye 28 days after treatment with digoxin, oleandrin, or proscillaridin.

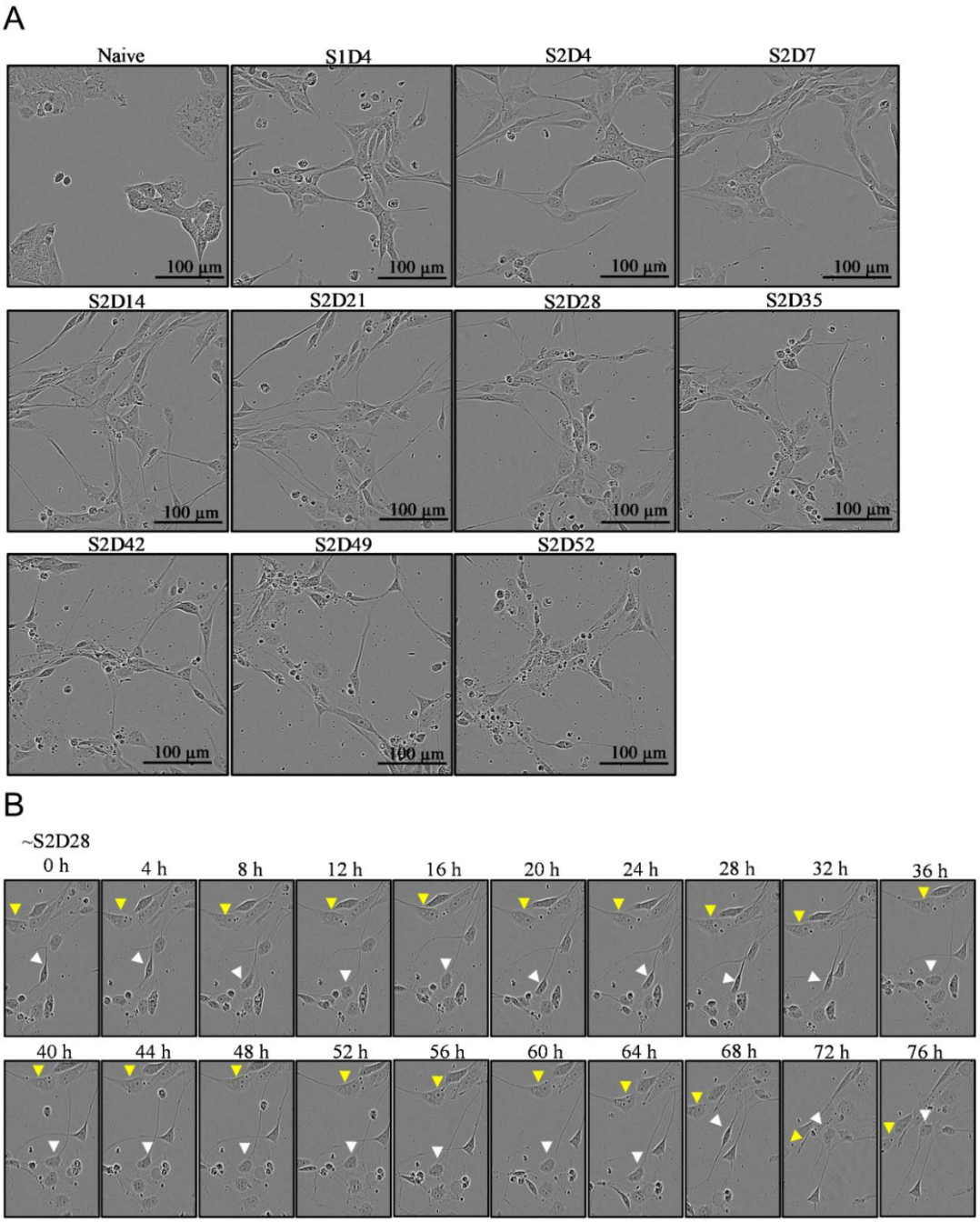

Supplementary Figure 3: PP121/bufalin promotes long-term differentiation into heterogeneous cell populations. (A) Representative images of cells over 8 weeks. The differentiation protocol completely blocked proliferation, and cells appeared healthy over 4 weeks and started to slowly degenerate after that. (B) Representative images showing a heterogeneous population. The white arrow pointed to motile, neuron-like cells with small cell bodies and neurite-like processes; the yellow arrow pointed to stationary, senescent-like cells with enlarged cell bodies and no processes.

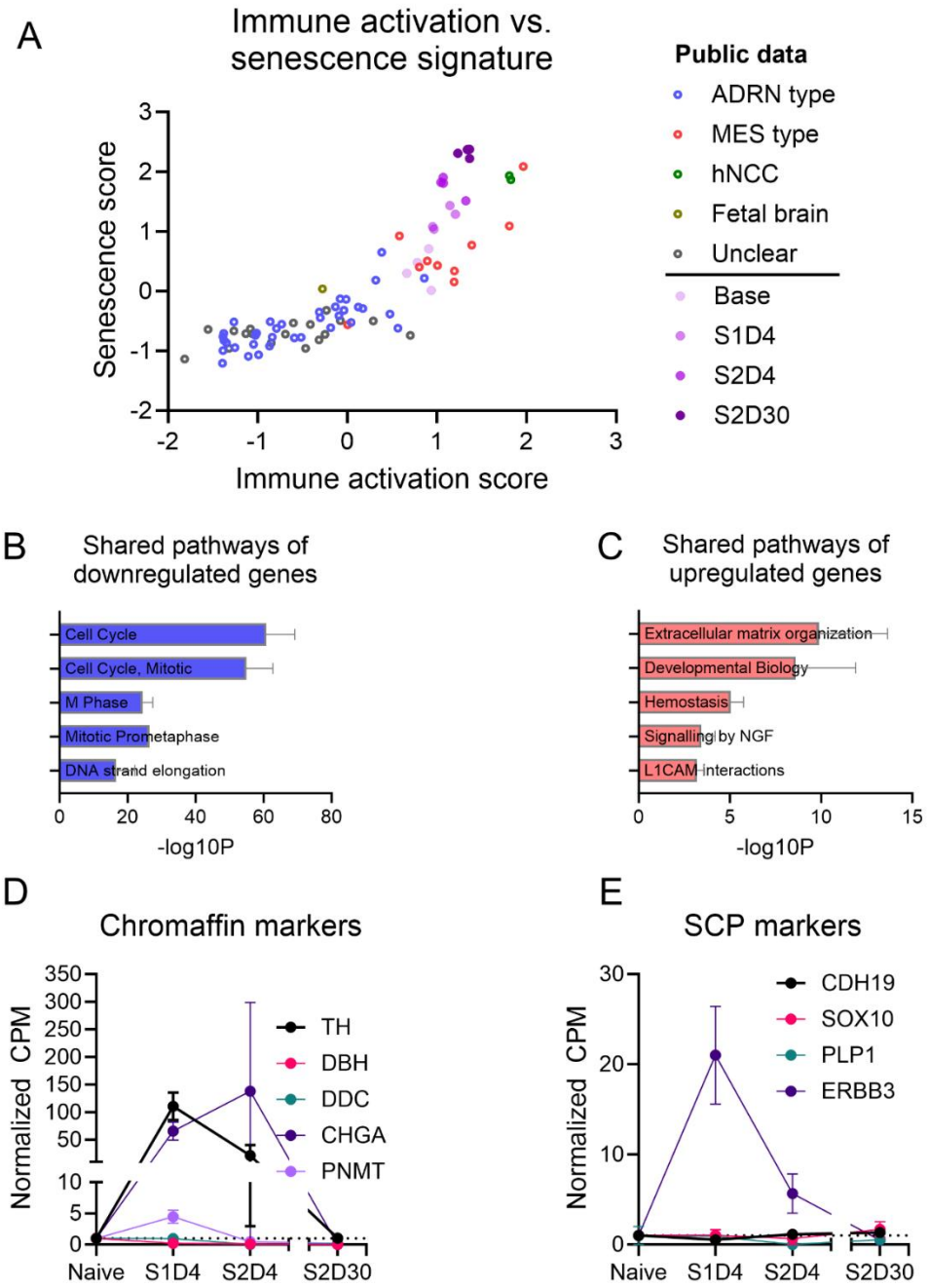

Supplementary Fig 4: PP121/bufalin-induced differentiation is distinct from RA-induced differentiation. (A) Differentiated SK-N-AS cells became increasingly more immune-activated and senescent (From public databases, N =67 samples; from this study, N =4 per group). **(B-C)** Shared pathways of up- and down-regulated genes between RA-differentiated BE2C, RA-differentiated NGP, and PP121/bufalin-differentiated SK-N-AS cells. **(D-E)** Markers associated with chromaffin cells and SCPs in naïve and differentiated SK-N-AS cells (N=4 per time point).

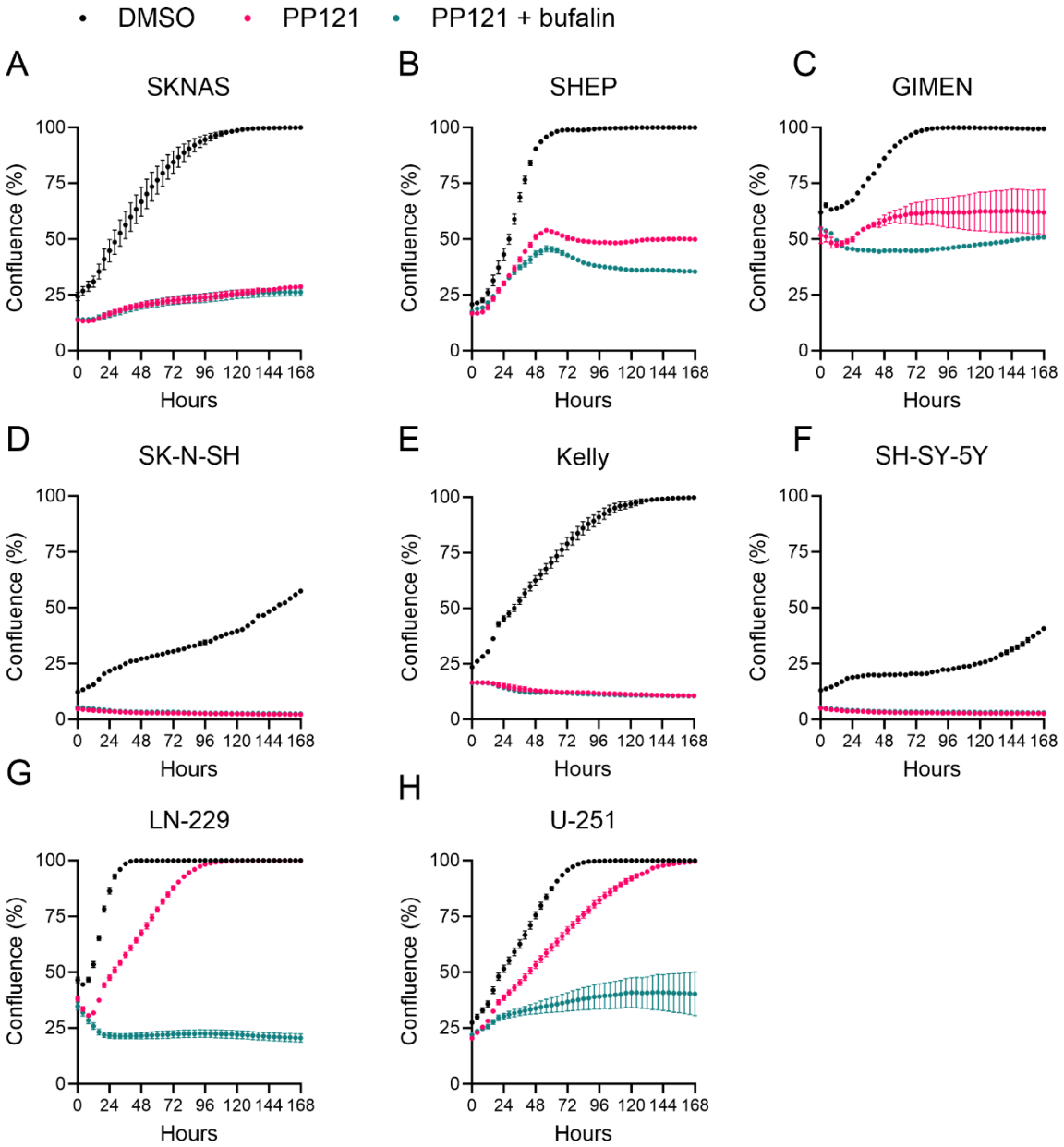

Supplementary Fig 5: Impact of PP121/bufalin on various cell lines. (A-C) PP121, with or without bufalin, was sufficient to completely inhibit the proliferation of MES neuroblastoma cells. **(D-F)** PP121, with or without bufalin, was sufficient to completely kill ADRN neuroblastoma cells. **(G-H)** PP121 alone slowed down but did not completely inhibit the proliferation of glioblastoma cell lines. PP121 with bufalin completely inhibited the proliferation of glioblastoma cell lines.

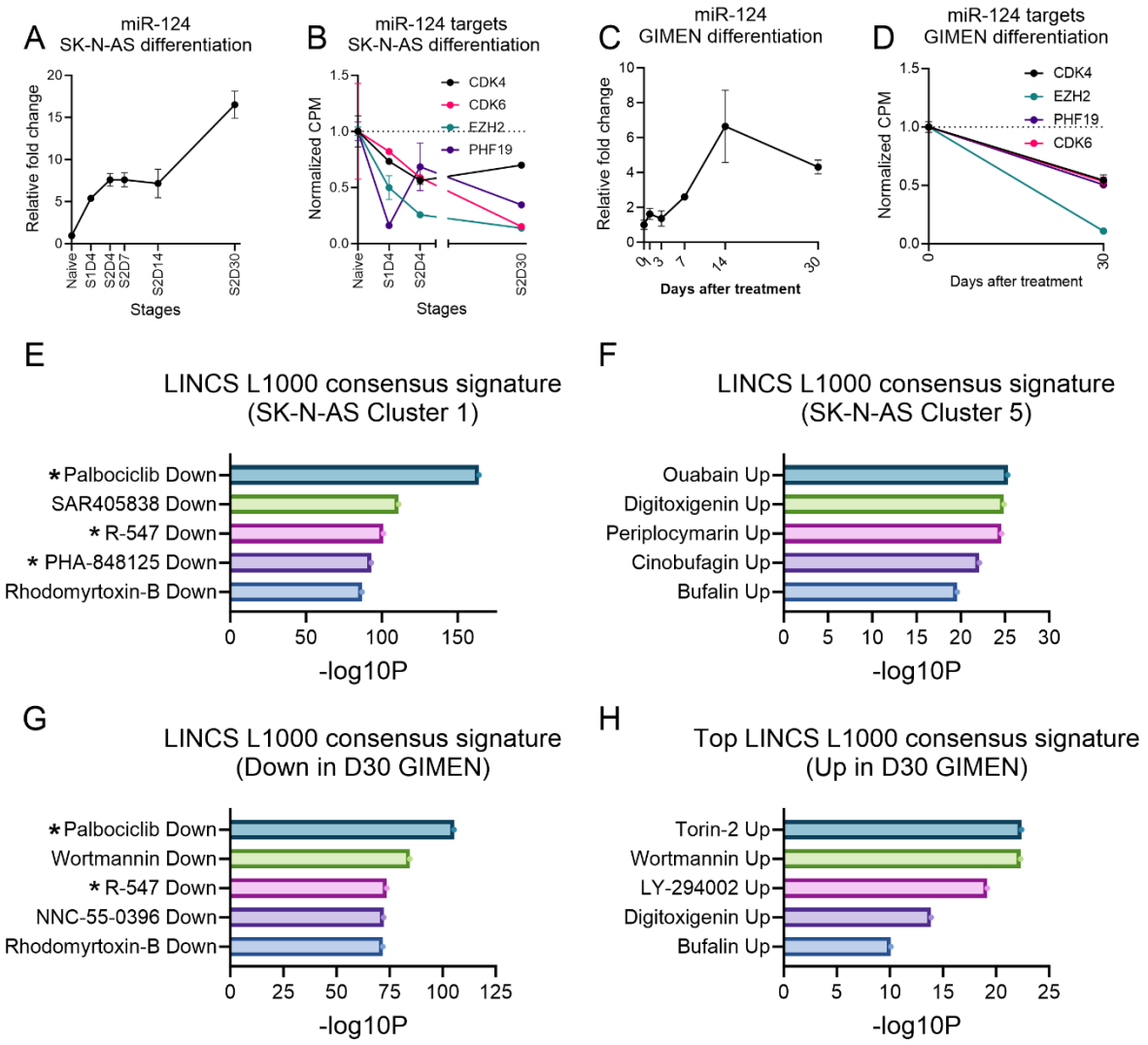

Supplementary Fig 6: miR-124 and drug signature in differentiated cells. (A-B) miR-124 was upregulated and some of its targets were downregulated in SK-N-AS cells. **(C-D)** Similar observations for GIMEN cells. **(E-H)** Consensus molecular drug signatures for various gene sets. Kinase inhibitors were specifically marked with *.

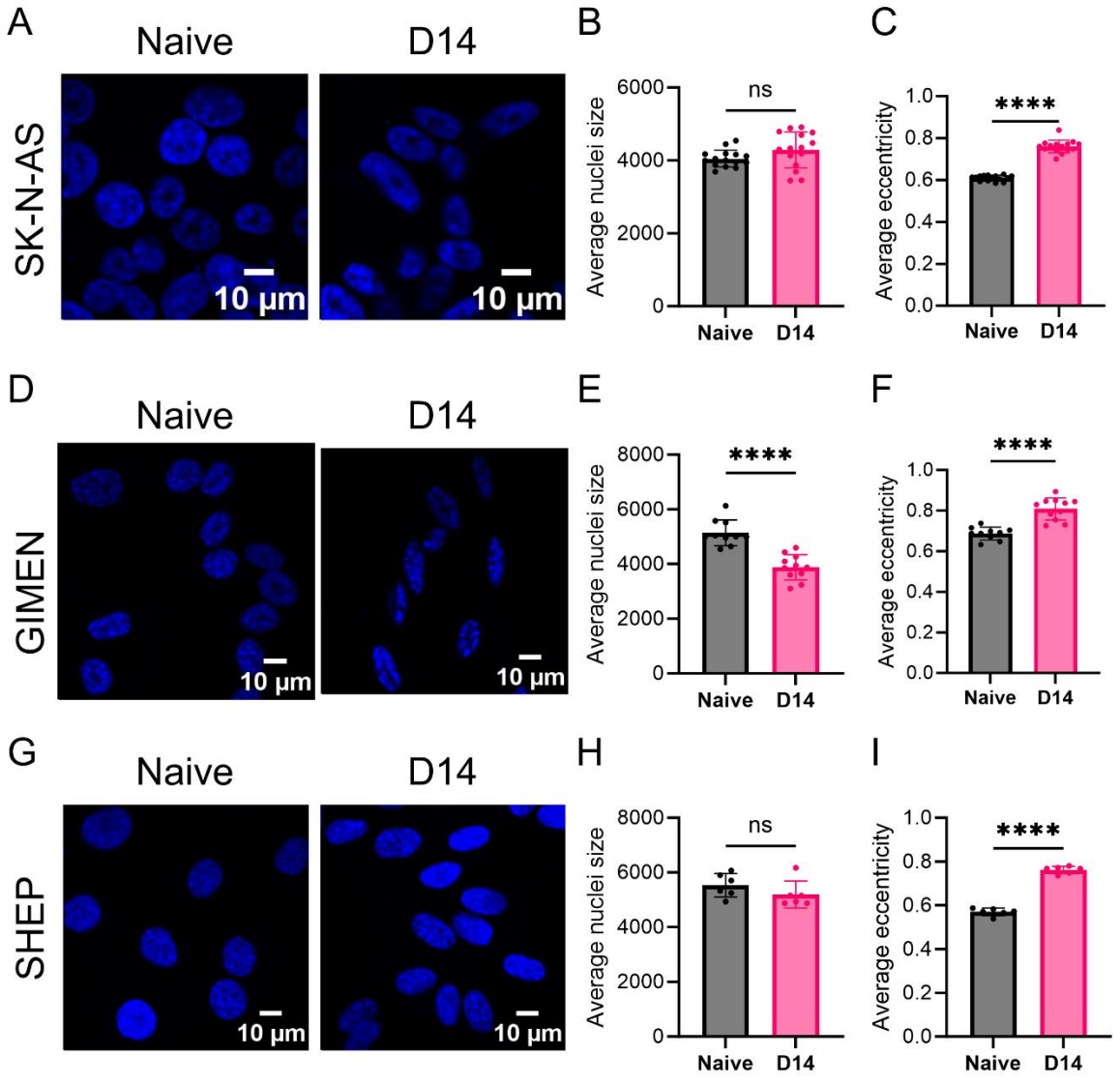

Supplementary Fig 7. Differentiation is associated with changes in nuclear morphology. (A-I) In all neuroblastoma cell lines tested, differentiation was associated with an elongation of the cell nuclei as measured by the increase in nuclei eccentricity.